J|A|C|S ARTICLES

Published on Web 12/11/2008

Equilibrium Electrostatics of Responsive Polyelectrolyte Monolayers

Kang Wang,[†] Rebecca A. Zangmeister,[‡] and Rastislav Levicky*,[†]

Department of Chemical and Biological Engineering, Polytechnic Institute of New York University, Brooklyn, New York 11201, and Process Measurements Division, National Institute of Standards and Technology, Gaithersburg, Maryland 20899

Received September 18, 2008; E-mail: rlevicky@poly.edu

Abstract: The physical behavior of polyelectrolytes at solid−liquid interfaces presents challenges both in measurement and in interpretation. An informative, yet often overlooked, property that characterizes the equilibrium organization of these systems is their membrane or rest potential. Here a general classification scheme is presented of the relationship between the rest potential and structural response of polyelectrolyte films to salt concentration. A numerical lattice theory, adapted from the polymer community, is used to analyze the rest potential response of end-tethered polyelectrolyte layers in which electrostatics and short-range contact interactions conspire to bring about different structural states. As an experimental quantity the rest potential is a readily accessible, nonperturbing metric of the equilibrium structure of a polyelectrolyte layer. A first set of measurements is reported on monolayers of end-tethered, single-stranded DNA in monovalent (NaCl) and divalent ($MgCl_2$) counterion environments. Intriguingly, in NaCl electrolyte at least two different mechanisms appear by which the DNA layers can structurally relax in response to changing salt conditions. In $MgCl_2$ the layers appear to collapse. The possible molecular mechanisms behind these behaviors are discussed. These studies provide insight into phenomena more generally underlying polyelectrolyte applications in the chemical, environmental, and biotechnological fields.

1. Introduction

Polyelectrolyte films at solid−liquid interfaces are encountered in fields ranging from the classical, such as water treatment and paper production,[1,2] to modern areas of nanotechnology and biotechnology where polyelectrolyte multilayers [3,4] and other assemblies [5−7] are used to precisely engineer surface properties. A fundamental challenge is to learn, from the complexity of interactions that a polyelectrolyte system may experience, which interactions dominate interfacial organization, under what experimental conditions, and whether the outcome assists or impairs functionality in applications. For example, in diagnostic applications[8−10] of DNA monolayers, interactions among DNA chains immobilized at the surface can bias their hybridization behavior toward analyte strands and thus complicate the interpretation of assay results.

Information on the structural state of a polyelectrolyte layer, at a flat solid−liquid interface, can be obtained through various in situ techniques sensitive to optical properties (e.g., ellipsometry,[11−13] neutron reflectivity,[14−16] total internal reflectance methods,[17,18] surface plasmon resonance[19,20]) or from force measurements (e.g., surface apparatus,[21,22] scanning probe methods[23−25]). In

[†] Polytechnic Institute of New York University.
[‡] National Institute of Standards and Technology.

(1) Faust, S. D.; Aly, O. M. *Chemistry of Water Treatment*, 2nd ed.; CRC Press LLC: Boca Raton, FL, 1998.
(2) Dautzenberg, H.; Jaeger, W.; Kotz, J.; Philipp, B.; Seidel, C.; Stscherbina, D. *Polyelectrolytes Formation, Characterization and Application*; Hanser: New York, 1994.
(3) *Multilayer Thin Films: Sequential Assembly of Nanocomposite Materials*; Decher, G., Schlenoff, J. B., Eds.; Wiley-VCH: Weinheim, Germany, 2003.
(4) Sukhishvili, S. A. *Curr. Opin. Colloid Interface Sci.* **2005**, *10*, 37–44.
(5) Bhat, R. R.; Tomlinson, M. R.; Wu, T.; Genzer, J. *Adv. Polym. Sci.* **2006**, *198*, 51–124.
(6) Ballauff, M. *Prog. Polym. Sci.* **2007**, *32*, 1135–1151.
(7) Ruhe, J.; et al. *Adv. Polym. Sci.* **2004**, *165*, 79–150.
(8) Schena, M.; Heller, R. A.; Theriault, T. P.; Konrad, K.; Lachenmeier, E.; Davis, R. W. *Trends Biotechnol.* **1998**, *16*, 301–306.
(9) Levicky, R.; Horgan, A. *Trends Biotechnol.* **2005**, *23*, 143–149.
(10) Graves, D. J. *Trends Biotechnol.* **1999**, *17*, 127–134.
(11) Kawaguchi, M.; Hayashi, K.; Takahashi, A. *Macromolecules* **1988**, *21*, 1016–1020.
(12) Biesalski, M.; Ruhe, J.; Johannsmann, D. *J. Chem. Phys.* **1999**, *111*, 7029–7037.
(13) Toomey, R.; Mays, J.; Tirrell, M. *Macromolecules* **2006**, *39*, 697–702.
(14) An, S. W.; Thirtle, P. N.; Thomas, R. K.; Baines, F. L.; Billingham, N. C.; Armes, S. P.; Penfold, J. *Macromolecules* **1999**, *32*, 2731–2738.
(15) Tran, Y.; Auroy, P.; Lee, L. T. *Macromolecules* **1999**, *32*, 8952–8964.
(16) Czeslik, C.; Jackler, G.; Hazlett, T.; Gratton, E.; Steitz, R.; Wittemann, A.; Ballauff, M. *Phys. Chem. Chem. Phys.* **2004**, *6*, 5557–5563.
(17) Sukhishvili, S. A.; Granick, S. *J. Chem. Phys.* **1998**, *109*, 6861–6868.
(18) Hansupalak, N.; Santore, M. M. *Macromolecules* **2004**, *37*, 1621–1629.
(19) Peterlinz, K. A.; Georgiadis, R. M.; Herne, T. M.; Tarlov, M. J. *J. Am. Chem. Soc.* **1997**, *119*, 3401–3402.
(20) Brockman, J. M.; Nelson, B. P.; Corn, R. M. *Annu. Rev. Phys. Chem.* **2000**, *51*, 41–63.
(21) Balastre, M.; Li, F.; Schorr, P.; Yang, J.; Mays, J. W.; Tirrell, M. V. *Macromolecules* **2002**, *35*, 9480–9486.
(22) Raviv, U.; Giasson, S.; Kampf, N.; Gohy, J. F.; Jerome, R.; Klein, J. *Nature* **2003**, *425*, 163–165.
(23) Biggs, S. *Langmuir* **1995**, *11*, 156–162.
(24) Cappella, B.; Dietler, G. *Surf. Sci. Rep.* **1999**, *34*, 1–104.
(25) Abbou, J.; Anne, A.; Demaille, C. *J. Am. Chem. Soc.* **2004**, *126*, 10095–10108.

10.1021/ja807435q CCC: $40.75

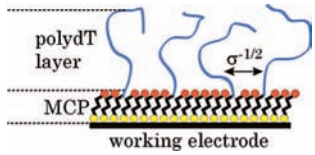

Figure 1. PolydT monolayers were prepared on gold working electrodes at various coverages, σ (strands/area). Mercaptopropanol (MCP) was used to block unoccupied regions of the electrode to suppress nonspecific adsorption of the polydT.

comparison electrochemical techniques, despite their real-time capability, excellent surface sensitivity, and access to structural information out of reach by other methods, have remained obscure as a tool for analysis of polyelectrolyte organization at interfaces. An especially useful intensive metric of the equilibrium structural state of a polyelectrolyte layer, and one which is readily measured electrochemically, is the membrane "Donnan" potential V_M, defined as the difference in electric potential between the interior of the film and the external electrolyte reservoir.[26−29]The experimental attractiveness of V_M as a structural probe is greatly enhanced by the fact that (1) these measurements do not need to supply energy to the sample and thus do not perturb the film organization from equilibrium, (2) V_M is readily measured under a broad range of conditions (e.g., salt valency and chemical identity, temperature, pH), and (3) real-time information is obtained, so that achievement of a stationary structure can be confirmed as data are acquired. The measurement itself is simple, with the minimal hardware requirement being a voltmeter.

The utility of membrane potential as a reporter on polyelectrolyte interfacial behavior depends on understanding how it relates to layer organization at the molecular level. In the present contribution this connection is developed for layers of end-immobilized, charged chains immersed in solutions of a single salt, a system that is nontrivial yet tractable, and which also encompasses a broad array of applications. Polyelectrolyte layers in which the chains are attached by one end as a monolayer to a solid−liquid interface[30] have served as smart surfaces and nanoactuators,[31] surface modifiers to tailor protein−surface interactions,[32,33] analyte-capture films in nucleic acid diagnostics,[9,10] and as vehicles for fundamental materials research.[7,34,35] After reviewing a general scheme for distinguishing classes of membrane potential behavior, the connection between V_M and layer structure is considered using numerical lattice calculations adapted from the polymer community.[36] The theoretical model serves both to validate "rules-of-thumb" for experimentally detecting specific types of V_M response and to extend understanding of select scenarios. This understanding is then applied to interpret experimental data from monolayers of polythymidylic acid single-stranded DNA, in solutions containing monovalent or divalent counterions.

2. Materials and Methods[37]

2.1. Sample Preparation. Experiments used single-stranded DNA of polythymidylic acid (polydT) of degree of polymerization $P = 10$ and 80, modified at the 3′ terminus with a disulfide moiety: dT_P-$(CH_2)_3$−S−S−$(CH_2)_3$−OH. A previously reported protocol,[38] following Herne and Tarlov,[39] was used to prepare mixed monolayers of end-anchored polydT strands embedded in a blocking layer of mercaptopropanol (MCP) (Figure 1). The MCP layer blocks nonspecific adsorption of nucleic bases to the support, leaving immobilized strands in an end-tethered geometry. Samples were prepared on 1.6 mm diameter polycrystalline gold electrodes that had been cleaned by mechanical polishing with 1 μm diamond polishing paste for 1 min, rinsed, and ultrasonicated in deionized (18.2 MΩ cm) water for 3 min, followed by electrochemical cleaning consisting of voltammetric cycling (−0.2 to 1.75 V, 0.1 V/s, 10 cycles) in 0.5 mol/L H_2SO_4. After a deionized water rinse, polydT was adsorbed onto the still-wetted electrodes from 1 μmol/L solutions in 1 mol/L NaCl, pH 7.0. Strand coverage, σ (chains/area), was controlled by varying the deposition time between 1 and 90 min. Following adsorption of polydT, samples were immersed in 1 mmol/L MCP in deionized water for 90 min, rinsed with deionized water, and used for rest potential measurements.

Samples for X-ray photoelectron spectroscopy (XPS) were prepared similarly but on gold-coated microscope slides of 5 nm Ti and 200 nm Au (Evaporated Metal Films, Ithaca, NY). After electrochemical polishing the slides were rinsed with deionized water, and the still-wetted surface was immersed in polydT and MCP deposition solutions as described above. A geometric area of 1.27 cm^2 was isolated on the slides by an O-ring seal clamped between the slide and an inverted glass tube. The tube also served as the sample cell with an approximate volume of 5 mL. Subsequent electrochemical and XPS measurements were performed within this area.

2.2. Determination of Strand Surface Coverages. Strand coverage was determined electrochemically based on a calibration of the reduction potential, E_R, of hexaamine-ruthenium (III) chloride ($RuHex^{3+}$) counterions, sequestered in polydT monolayers,[40−43] against nominally absolute values determined from XPS.[38] E_R is a function of polydT coverage because of (i) a coverage-dependent membrane potential at the layer−electrolyte boundary [38,44] and, (ii) dependence of electron transport reversibility on layer thickness and crowding, especially for thicker $P = 80$ films. To establish the calibration, polydT monolayers were prepared on gold-coated glass slides and a baseline cyclic voltammetry (CV) scan was measured in 10 mmol/L NaCl, pH 7.0 ± 0.1, at room

(26) Donnan, F. G. *J. Membr. Sci.* **1995**, *100*, 45–55.
(27) Naegeli, R.; Redepenning, J.; Anson, F. C. *J. Phys. Chem.* **1986**, *90*, 6227–6232.
(28) Doblhofer, K.; Armstrong, R. D. *Electrochim. Acta* **1988**, *33*, 453–460.
(29) Buck, R. P.; Vanysek, P. *J. Electroanal. Chem.* **1990**, *292*, 73–91.
(30) Miklavic, S. J.; Marcelja, S. *J. Phys. Chem.* **1988**, *92*, 6718–6722.
(31) Zhou, F.; Huck, W. T. S. *Phys. Chem. Chem. Phys.* **2006**, *8*, 3815–3823.
(32) Tran, Y.; Auroy, P.; Lee, L. T.; Stamm, M. *Phys. Rev. E* **1999**, *60*, 6984–6990.
(33) Kusumo, A.; Bombalski, L.; Lin, Q.; Matyjaszewski, K.; Schneider, J. W.; Tilton, R. D. *Langmuir* **2007**, *23*, 4448–4454.
(34) Ballauff, M.; Borisov, O. *Curr. Opin. Colloid Interface Sci.* **2006**, *11*, 316–323.
(35) Tirrell, M.; Levicky, R. *Curr. Opin. Solid State Mat. Sci.* **1997**, *2*, 668–672.
(36) Scheutjens, J. M. H. M.; Fleer, G. J. *J. Phys. Chem.* **1979**, *83*, 1619–1635.
(37) Certain commercial equipment, instruments, or materials are identified in this report to specify adequately the experimental procedure. Such identification does not imply recommendation or endorsement by the National Institute of Standards and Technology, nor does it imply that the materials or equipment identified are necessarily the best available for the purpose.
(38) Shen, G.; Tercero, N.; Gaspar, M. A.; Varughese, B.; Shepard, K.; Levicky, R. *J. Am. Chem. Soc.* **2006**, *128*, 8427–8433.
(39) Herne, T. M.; Tarlov, M. J. *J. Am. Chem. Soc.* **1997**, *119*, 8916–8920.
(40) Steel, A. B.; Herne, T. M.; Tarlov, M. *J. Anal. Chem.* **1998**, *70*, 4670–4677.
(41) Steel, A. B.; Herne, T. M.; Tarlov, M. J. *Bioconjugate Chem.* **1999**, *10*, 419–423.
(42) Su, L.; Sankar, C. G.; Sen, D.; Yu, H. Z. *Anal. Chem.* **2004**, *76*, 5953–5959.
(43) Yu, H.-Z.; Luo, C.-Y.; Sankar, C. G.; Sen, D. *Anal. Chem.* **2003**, *75*, 3902–3907.
(44) Ceres, D. M.; Udit, A. K.; Hill, H. D.; Hill, M. G.; Barton, J. K. *J. Phys. Chem. B* **2007**, *111*, 663–668.

temperature (22 ± 1 °C), followed by a scan in 1 μmol/L $RuHex^{3+}$, in the same electrolyte, after a 10 min wait time. All CVs were run at 0.08 V/s, from 0 to −0.45 V vs an Ag/AgCl/3mol/L NaCl reference (Bioanalytical Sciences; 0.209 V vs NHE at 25 °C). A platinum wire served as the counter electrode. Electrolyte solutions were deoxygenated prior to each measurement by bubbling high purity nitrogen through the solutions for 10 min. Following CV measurements samples were immersed for 5 min in 1 mol/L $MgCl_2$, followed by 5 min immersion in 1 mol/L NaCl, and a final rinse with deionized water to remove polydT-complexed RuHex. The samples were dried and strand coverage was determined with XPS.

XPS was performed at the National Institutes of Standards and Technology, Gaithersburg, MD, on a Kratos Axis Ultra DLD instrument with a hemispherical analyzer, a monochromatic Al Kα (1486.7 eV) source, a 90° takeoff angle, a 40 eV pass energy, and a 300 μm × 700 μm analysis area. Strand coverages were calculated from the ratio of the integrated intensity of the P 2p emission band at 134 eV of polydT to that of the Au 4f band from the solid support at 84 eV ($4f_{7/2}$) plus at 88 eV ($4f_{5/2}$). Details of data processing and calculation are provided in the Supporting Information and follow previously reported methods.[38,45] Two nonoverlapping spots were characterized for each sample; their average was used in all subsequent calculations. Coverages were corrected for surface roughness which was estimated from the relative XPS intensity of S 2p to Au 4f lines, taking 4.67×10^{14} S atoms to be present per 1 cm^2 of Au surface.[46,47] This yielded a roughness factor, representing the ratio of true to geometric areas, of 1.13 ± 0.05 (seven samples). The final calibration, in the form of an E_R vs σ plot, was used to determine σ directly from E_R data.

PolydT 80mer samples could be measured to lower coverages, in terms of strands/area, than 10mers because of their stronger P 2p XPS signal per strand. However, 80mer samples could not be prepared at as high a coverage as 10mers because their polymeric nature limited the packing density.

2.3. Rest Potential Measurements. Experiments do not directly measure the membrane potential V_M; rather, they provide the rest potential V_R defined as the stabilized value of the open-circuit potential of the polydT-modified working electrode relative to the reference electrode. As discussed later, trends in V_R closely track changes in the membrane potential; thus, changes in V_R were interpreted as corresponding to those in V_M. Rest potential measurements were performed on a CH Instruments electrochemical workstation (CHI 660C) with a two-electrode configuration consisting of a DNA-modified 1.6 mm working electrode and an AgCl/Ag wire that served as a combined reference/counter electrode. Use of the Ag/AgCl wire avoided liquid junction biases that arise with conventional reference electrodes. The same wire was used for all measurements. Measurements were performed in deoxygenated NaCl or $MgCl_2$ solutions, adjusted to pH 7.0 with HCl or NaOH immediately prior to experiments. Each experiment consisted of monitoring the open circuit potential (OCP) as a function of time for up to 30 min.

Rest potentials were subsequently referenced to an Ag/AgCl/3mol/L NaCl "standard" through the Nernst equation and empirical electrolyte mean activity coefficients, $y_\pm$, taken from the literature.[48] The offset, ΔE, between the Ag/AgCl wire and the Ag/AgCl/3 mol/L NaCl reference follows from $\Delta E = (kT/e)\ln(a_{3M}^{Cl^-}/a^{Cl^-})$, where $a^{Cl^-} = y_- C^{Cl^-}$ is the activity of Cl^- at concentration C^{Cl^-}, y_- is the activity coefficient, k is the Boltzmann constant, T is the absolute temperature, and e is the elementary charge. The individual anionic and cationic activities were estimated from $y_\pm$ using the Debye−Hückel relationship $y_+^{1/q_+^2} = y_-^{1/q^2}$ and the definition $y_\pm = y_+^{\nu_+/\nu} y_-^{\nu_-/\nu}$, where q_+ and q_- are cationic and anionic valencies, ν_+ and ν_- are the moles of cations and anions per mole of salt, and $\nu = \nu_+ + \nu_-$.

2.4. Calculation of Rest Potentials from Lattice Theory. A lattice theory approach was implemented to explore general features of the relationship between rest potential and organization of a polyelectrolyte layer. The rest potential can be found by minimizing the free energy per area, A, of the region that includes and is bound by the working electrode on one side, and by the electrolyte solution on the other

$$\frac{\partial A}{\partial V_S} = 0 \quad \text{at} \quad V_S = V_R \tag{1}$$

V_S is the potential difference between the electrode and bulk electrolyte. Equation 1 was solved by calculating A as a function of V_S, using the self-consistent-field lattice theory of Scheutjens and Fleer (SF)[36,49] extended to polyelectrolyte systems.[50,51] SF theory has achieved considerable success in elucidating equilibrium interfacial behavior of polymers,[52] motivating its present extension to equilibrium electrochemical properties of these systems. Modeling of electrochemical properties based on a molecular-level structural description of an interface has an especially strong history in the case of redox-active layers, for example in theories applicable to self-assembled monolayers[53−55] and electroactive polymer films.[56−60] In such situations there is an imposed surface condition—potential or charge—and any structural equilibration that occurs is subject to this condition. In comparison, in the calculation of rest potential neither surface potential nor charge are known a priori. Instead, these quantities are determined by minimization of the overall system free energy, including that of the electrode.

SF theory accounts for constraints of volume conservation $\sum_i \phi_i = 1$ (ϕ_i, volume fraction of species i), connectivity of chain segments, geometry of chain immobilization, and self-consistency of the spatial distribution of charged species with the electrostatic potential. Its key simplifications, as implemented, include inclusion of self-intersecting chain configurations, treatment of layer structure as uniform parallel to the solid support, neglect of molecular details specific to a particular polyelectrolyte (e.g., chain flexibility), and equivalency of cation, anion, solvent, and chain segment volumes. The simplification to a laterally smeared charge distribution removes image charge effects.[54,61,62] Subject to these approximations the theory provides the z-dependence of layer properties (e.g., z-direction profiles for $\{\phi_i\}$ and V), where z is the perpendicular distance from the solid support.

Mathematical details of the model and solution methodology are provided in the Supporting Information. The lattice consisted of

(45) Petrovykh, D. Y.; Kimura-Suda, H.; Tarlov, M. J.; Whitman, L. J. *Langmuir* **2004**, *20*, 429–440.
(46) Strong, L.; Whitesides, G. M. *Langmuir* **1988**, *4*, 546–558.
(47) Johnson, P. A.; Levicky, R. *Langmuir* **2004**, *20*, 9621–9627.
(48) Robinson, R. A.; Stokes, R. H. *Electrolyte Solutions*, 2nd ed.; Dover Publications: Mineola, NY, 1959.
(49) Cosgrove, T.; Heath, T.; van Lent, B.; Leermakers, F. A. M.; Scheutjens, J. M. H. M. *Macromolecules* **1987**, *20*, 1692–1696.
(50) Bohmer, M. R.; Evers, O. A.; Scheutjens, J. M. H. M. *Macromolecules* **1990**, *23*, 2288–2301.
(51) Israels, R.; Leermakers, F. A. M.; Fleer, G. J.; Zhulina, E. B. *Macromolecules* **1994**, *27*, 3249–3261.
(52) Fleer, G. J.; Stuart, M. A. C.; Scheutjens, J. M. H. M.; Cosgrove, T.; Vincent, B. *Polymers at Interfaces*; Chapman and Hall: London, 1993.
(53) Smith, C. P.; White, H. S. *Anal. Chem.* **1992**, *64*, 2398–2405.
(54) Andreu, R.; Calvente, J. J.; Fawcett, W. R.; Molero, M. *Langmuir* **1997**, *13*, 5189–5196.
(55) Ohtani, M.; Kuwabata, S.; Yoneyama, H. *Anal. Chem.* **1997**, *69*, 1045–1053.
(56) Bowden, E. F.; Dautartas, M. F.; Evans, J. F. *J. Electroanal. Chem.* **1987**, *219*, 49–69.
(57) Chidsey, C. E. D.; Murray, R. W. *J. Phys. Chem.* **1986**, *90*, 1479–1484.
(58) Lizarraga, L.; Andrade, E. M.; Florit, M. I.; Molina, F. V. *J. Phys. Chem. B* **2005**, *109*, 18815–18821.
(59) Posadas, D.; Fonticelli, M.; Presa, M. J. R.; Florit, M. I. *J. Phys. Chem. B.* **2001**, *105*, 2291–2296.
(60) Tagliazucchi, M.; Calvo, E. J.; Szleifer, I. *Langmuir* **2008**, *24*, 2869–2877.
(61) MacDonald, J. R.; Barlow, C. A. *J. Electrochem. Soc.* **1966**, *113*, 978–992.
(62) Wittmer, J.; Joanny, J. F. *Macromolecules* **1993**, *26*, 2691–2697.

Table 1. Parameters Used in Lattice Theory Calculations

parameter	value	parameter	value
$\chi_{i,j} = \chi_{j,i}$ [a]	−100 to 8	σ (chains/cm^2)	2×10^{12} to 2.1×10^{13}
$\varepsilon_{\text{chain}}$	2.0	N	10−80
$\varepsilon_{\text{cation}}$, $\varepsilon_{\text{anion}}$, $\varepsilon_{\text{solvent}}$	80	ε_{P} [b]	5.0
T (K)	300	t_{P} [b] (nm)	0.7
C_{B} (mol/L)	0.01−1	q_+	+1
q_-	−1	q_{chain} [c]	−1

[a] $\chi_{i,j}$ of 1 corresponds to a cost of 1 kT for transferring species i from pure i to pure j. [b] These values correspond to an MCP passivation monolayer, taken from ref 38. [c] Valence of one chain segment.

the working electrode surface (layer number "−1"), a surface passivation layer of thickness, t_{P} (layer 0), with properties corresponding to those of an MCP monolayer, and layers 1 through M containing the polyelectrolyte film and a portion of the electrolyte solution. The last layer, layer M, was chosen to be sufficiently away from the surface so that the electrostatic potential $V(z)$ decayed by at least 5 orders of magnitude from its maximum in the film. In layers 1 through M, chain configurations were generated on a cubic lattice with a cell volume d^3 equal to 0.53 nm^3, yielding $d = 0.81$ nm. The maximum chain coverage in the lattice model is $1/d^2$, or 1.5×10^{14} chains/cm^2. The segments of a chain were connected in series, with the first segment anchored to the surface. The bonds between segments were fully flexible, meaning that at each segment a chain could proceed in any of the directions afforded by the lattice.

The calculation proceeds from an initial guess for the energies of each species (cation, anion, solvent, or chain segment) in each of the layers 1 to M. The energies include a hard-core interaction that is the same for all species, contact interactions between species i and j and, for charged species, electrostatic energy due to a nonzero local potential, V.[50,51] The hard-core interaction is adjusted in each layer to enforce incompressibility ($\sum_i \phi_i = 1$). Boltzmann statistics are used to calculate the z-dependent probabilities of each species from the energies, with the probability of a chain configuration determined by the product of segmental probabilities reflecting the number of segments in each lattice layer for that configuration. The probabilities are normalized so that cation, anion, and solvent volume fractions approach bulk values away from the surface, and chain coverage is equal to the input value. From the resultant volume fractions the contact and electrostatic energies are updated, new Boltzmann factors are obtained, and the calculation is repeated until convergence. Parameters that determine A include chain coverage, σ, number of segments per chain, N, concentration of salt in bulk solution, C_{B}, specie valencies, q_i, interaction energies (Flory parameters[36]) χ_{ij} between i and j species (i and j include chain segments, cations, anions, solvent, and surface sites), temperature, T, dielectric constants, ε_i, and thickness of the passivation layer, t_{P}. The ranges used for these parameters are listed in Table 1. The calculations are implemented under the common electrochemical situation of an imposed surface potential V_{S}. Following eq 1 free energy, A, is calculated as a function of V_{S}, and V_{R} is determined from the minimum of the $A-V_{\text{S}}$ curve as illustrated in Figure 2.

3. Results and Discussion

3.1. Classes of Rest Potential Behavior. When a polyelectrolyte layer is exposed to a change in conditions, the most rudimentary question is how the organization of the layer adjusts. Rest potential measurements can address this point. For clarity, the polyelectrolyte is assumed to be negatively charged, and immersed in electrolyte with a single type of salt. The salt cations and polyelectrolyte counterions are identical. At equilibrium the electrochemical potentials of partitioning ions

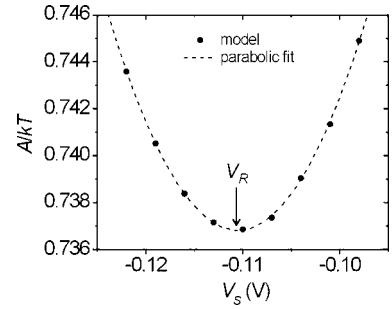

Figure 2. Rest potential, V_{R}, corresponds to the minimum in free energy, A, following eq 1. A parabolic fit (dashed line) was used to interpolate between theoretically calculated values (points).

between the solution and the film must be equal, e.g., for cations this yields the familiar result[26,28,63]

$$\mu^{\text{cat,o}} + kT \ln(a_{\text{F}}^{\text{cat}}) + q_+ e V_{\text{M}} = \mu^{\text{cat,o}} + kT \ln(a_{\text{B}}^{\text{cat}})$$

where $\mu^{\text{cat,o}}$ is the cation chemical potential in the reference state, $a_{\text{F}}^{\text{cat}}$ is the cation activity in the film, $a_{\text{B}}^{\text{cat}}$ is the cation activity in solution, and V_{M} is the membrane potential relative to solution. The above equation rearranges to

$$V_{\text{R}} \approx V_{\text{M}} = \frac{kT}{q_+ e} \ln\left[\frac{a_{\text{B}}^{\text{cat}}}{a_{\text{F}}^{\text{cat}}}\right] = \frac{2.303kT}{q_+ e} \log\left[\frac{a_{\text{B}}^{\text{cat}}}{a_{\text{F}}^{\text{cat}}}\right] \qquad (2)$$

where the rest potential V_{R} was set equal to the membrane (Donnan) potential, V_{M}, thus removing contributions from potential changes other than between the polyelectrolyte film and solution. This approximation will be examined below in more detail.

Three general types of behavior can be anticipated. First, at sufficiently high salt concentrations the membrane potential is strongly screened and V_{R} approaches zero. From eq 2, in this limit $a_{\text{B}}^{\text{cat}}$ approaches $a_{\text{F}}^{\text{cat}}$ or, if ideal behavior applies, $C_{\text{B}}^{\text{cat}}$ approaches $C_{\text{F}}^{\text{cat}}$ with concentrations replacing activities. This regime will be referred to as the salt-dominated (SD) regime. Within the SD regime the electrostatic work of transferring a counterion from solution to the layer, across V_{R}, is comparable to or less than thermal energy, kT. The threshold condition for onset of the SD regime can therefore be stated as

$$|q_+ e V_{\text{R}}| = kT \qquad (3)$$

For example, for monovalent counterions and ambient conditions eq 3 predicts that, at the onset of the SD regime, $|V_{\text{R}}| = |kT/q_+ e| \approx 0.025$ V. Since the other bound on V_{R}, in the limit of very high salt, is 0, the width of the SD regime for monovalent counterions is predicted to span a 0.025 V change in V_{R}.

At lower salt concentrations, outside the SD regime, $a_{\text{F}}^{\text{cat}} > a_{\text{B}}^{\text{cat}}$ and two general types of behavior are expected based on whether the polyelectrolyte film responds to changes in salt concentration. In the unresponsive (U) state, the polyelectrolyte layer is insensitive to variations in solution salt concentration. The layer structure and therefore concentration of polyelectrolyte charge do not vary with the level of external salt. The cation concentration in the film, and hence activity, $a_{\text{F}}^{\text{cat}}$, can then also be approximated as constant. In this case eq 2 predicts that V_{R} will change linearly with $\log a_{\text{B}}^{\text{cat}}$, with a slope of $2.303kT/q_+ e$ (0.059 V at 300 K).[26−28] U behavior has been experimentally documented through shifts in the redox potential of electroactive

(63) Buck, R. P. *Anal. Chem.* **1968**, *40*, 1432–1439.

couples incorporated into charged surface layers, including into Nafion coatings,[27] polyelectrolyte multilayers,[64] DNA monolayers,[44,65] and other systems of high interfacial charge.[66] Alternately, in the salt-responsive (SR) regime the polyelectrolyte layer responds to changes in salt concentration by readjusting its structure; for example, by swelling or by changing the extent of ionization of the chains. The direction of the response in layer organization is expected to relax, and diminish, the adjustment in V_R that would arise had the film been unresponsive.

Since both SR and SD behaviors are expected to manifest as a weakened dependence (relative to a U-type relationship) of V_R on log a_B^{cat}, it may be difficult to distinguish from experimental data which behavior dominates. One way to decide whether SR behavior is significant is suggested by eq 3. Equation 3 predicts that, in the SD regime, the absolute magnitude of V_R is limited to between 0 and $|kT/q_+e|$; thus, observation of deviations from U behavior over a range significantly wider than $|kT/q_+e|$ would signify a responsive system.

3.2. Comparison to Lattice Theory. The general characteristics of rest potential response, as outlined above, were examined for the specific geometry of a layer of end-tethered polyelectrolyte chains through lattice model calculations. Since polyelectrolyte molecules can exhibit both attractive (e.g., hydrophobic) and repulsive (e.g., electrostatic) interactions between segments, an added goal of the calculations was to consider the interplay of segment−segment attractions and repulsions as manifested in V_R data. In the lattice model, short-range contact interactions are represented by the parameters $\chi_{i,j}$, where a positive value is a penalty (i.e., a repulsion) for contacts between species i and j. Interactions between all solution species were set to zero, while those between polyelectrolyte segments and solution species (i.e., $\chi_{chain,cation}$, $\chi_{chain,anion}$, $\chi_{chain,solvent}$) were assigned a common value of χ (dropping the subscripts). χ can thus be viewed as a preference ($\chi > 0$) or aversion ($\chi < 0$) for chain−chain over chain−solution contacts. All interactions with the solid support were assigned a value of 0.

Figure 3 shows examples of layer properties calculated at the equilibrium condition when surface potential equals V_R. Since the chains are negatively charged the layer preferentially accumulates cations and expels anions; this permselectivity is evident in Figure 3A where the volume fractions of both species are plotted as a function of distance from the surface. In Figure 3B, the net charge per area, given by $\sum_i q_i e\phi_i(z)/d^2$, exhibits a positive region around $z = 9$ nm. The accumulation of positive charge is due to leaking of counterions outside the confines of the layer, leaving it with an overall negative charge in the distance range 1 nm $< z <$ 7 nm. The resultant charge separation produces the membrane potential V_M. The structuring close to the surface derives from a layering of cations and chain segments in this region. Figure 3C plots the potential profile $V(z)$, which decreases from solution into the negatively charged layer. As indicated in the figure, the difference between V_R and V_M consists of the potential drop across the passivation layer. For the selected parameters of the passivation layer (Table 1), representative of an MCP film, the equilibrium value of this potential drop was ~1 mV and therefore small in comparison

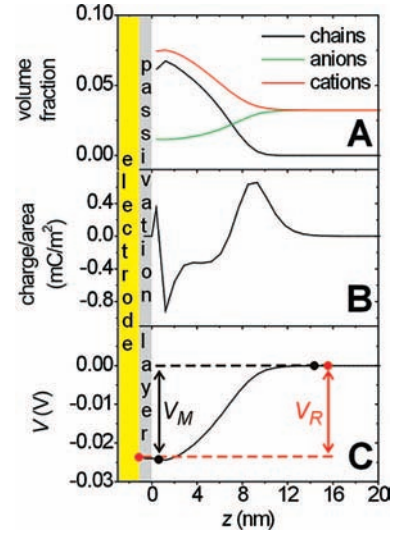

Figure 3. (A) Volume fraction of chain segments, anions, and cations as a function of the distance z from the solid support. The interface between the passivation layer and the polyelectrolyte film is at $z = 0$. (B) Net charge per area as a function of z. (C) Corresponding potential profile. All graphs share a common z-axis scale. Parameters: $\sigma = 3.7 \times 10^{12}$ chains/cm^2; $N = 20$; $C_B = 0.1$ mol/L; $\chi_{i,j} = 0$ for all i,j; $d = 0.81$ nm; other parameters as in Table 1. Gray area indicates the passivation layer; yellow area corresponds to the Au working electrode.

to the membrane potential V_M, supporting the approximation $V_R \approx V_M$ in eq 2.

Rest potentials were calculated as a function of chain length, N, salt concentration, C_B, chain coverage, σ, and contact interactions, χ. Figure 4 summarizes results for layers with $N = 10$ and χ between −100 and 8, and for several chain coverages as indicated in the caption (higher coverages correspond to heavier line widths). These chain coverages represent modestly crowded layers. For example, 1×10^{13} chains/cm^2 corresponds to a chain−chain spacing of about 3 nm, what can be compared to an 8 nm end-to-end distance for a fully stretched 10mer chain. Parts A and B of Figure 4 consider the unlikely but illustrative $\chi = -100$ scenario. For this χ chain−chain contacts are highly repulsive, resulting in a strongly swollen film whose structure is determined by a balance between chain stretching and contact interactions. With electrostatics only a weaker contribution, the layer does not respond significantly to salt concentration; accordingly, for a given chain coverage, all profiles from 0.01 to 1 mol/L salt overlap in Figure 4B. Since the layer is unresponsive to salt, only the SD and U regimes should be observed. Indeed, as C_B decreases the slopes for all three coverages in Figure 4A approach the limiting U value of 0.059 V per decade, indicated by the purple guidelines. The horizontal dashed line represents the predicted SD onset at $|V_R| = |kT/q_+e| \approx 0.025$ V, following eq 3. The criterion is seen to reasonably separate the U and SD regimes. Above the threshold, in the SD regime, as salt concentration increases the membrane potential is suppressed and V_R approaches 0.

Increasing χ from −100 in the positive direction reduces repulsions between chains and allows the layer to contract to a less stretched state. Contraction of the film concentrates its negative charge and hence leads to more negative rest potentials. These changes in V_R are illustrated in Figure 4C for coverages of 1.4×10^{13} (lighter lines) and 2.1×10^{13} chains/cm^2 (heavier lines). At lower salt concentrations the $\chi = 0$ and 4 films exhibit U behavior. However, as salt increases deviations from the limiting U slope occur earlier, and it is evident from the $\chi = 4$

(64) Calvo, E. J.; Wolosiuk, A. *J. Am. Chem. Soc.* **2002**, *124*, 8490–8497.
(65) Boon, E. M.; Jackson, N. M.; Wightman, M. D.; Kelley, S. O.; Hill, M. G.; Barton, J. K. *J. Phys. Chem. B* **2003**, *107*, 11805–11812.
(66) Redepenning, J.; Tunison, H. M.; Finklea, H. O. *Langmuir* **1993**, *9*, 1404–1407.

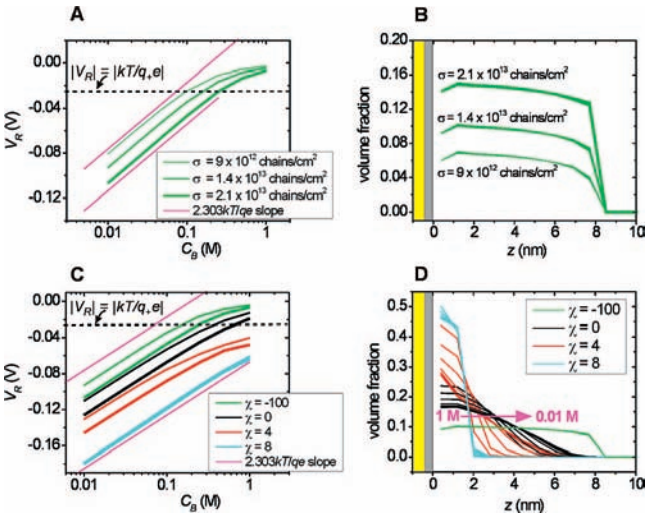

Figure 4. Trends in rest potential for $N = 10$ films calculated from lattice theory. (A) V_R as a function of salt concentration for an unresponsive layer; $\chi = -100$. Results are shown for three different chain coverages. (B) Chain volume fraction profiles for films whose V_R response is plotted in (A). For these unresponsive layers, the volume fraction profiles, at a given chain coverage, overlap as C_B varies from 0.01 to 1 mol/L. (C) V_R as a function of salt concentration for different settings of χ. Line thickness corresponds with chain density (e.g., thicker lines are for $\sigma = 2.1 \times 10^{13}$ chains/cm^2; thinner lines for $\sigma = 1.4 \times 10^{13}$ chains/cm^2). (D) Volume fraction profiles corresponding to coverage $\sigma = 1.4 \times 10^{13}$ chains/cm^2 in part (C). For each χ, profiles are shown for salt concentrations of 0.01, 0.025, 0.05, 0.1, 0.25, 0.5, and 1 mol/L. Salt concentration has little influence on the profiles when chain−chain contact interactions are either strongly repulsive ($\chi = -100$, green lines) or strongly attractive ($\chi = 8$, blue lines). In (A) and (C) purple lines represent the unresponsive limit, while horizontal dashed lines demark onset of the SD regime.

data that deviations can arise well before onset of the SD regime. These deviations are a signature that the polyelectrolyte layer is responsive to salt. The origins of the responsive behavior are evident from the volume fraction profiles in Figure 4D. Considering the $\chi = 4$ profiles (red traces) in Figure 4D, at low salt concentrations the film is swollen by electrostatic repulsions between chains and the volume fraction profiles superpose. However, as C_B is increased from 0.01 to 1 mol/L, the layer starts to contract. The contraction increases the counterion concentration in the layer so as to partially match the increase in solution salt. This lowers the sensitivity of the rest potential to changes in C_B (e.g., see eq 2) and causes deviations from the U limit. The deviations are more pronounced for $\chi = 4$ (red lines in Figure 4C) than $\chi = 0$ (black lines in Figure 4C) because, for $\chi = 4$, stronger chain−chain attractions cause a more complete collapse and thus a stronger response of the layer as salt concentration increases.

Increasing χ to $\chi = 8$ resulted in a loss of responsive behavior and caused a U type linear relationship between V_R and log C_B (blue curves in Figure 4C). The origin of this unresponsive behavior can be identified from the corresponding volume fraction profiles (Figure 4D) which show that the layer exists as a collapsed film over the entire salt range. This suggests a further subdivision of unresponsive behavior for polyelectrolyte films into unresponsive stretched (US) and unresponsive collapsed (UC) states. US behavior applies when chain stretching is close to saturation, i.e., as in the $\chi = -100$ scenario. In contrast UC behavior arises from overwhelmingly attractive contacts between chains, as for $\chi = 8$, that cause the layer to precipitate into a structure that is insensitive to salt variations. Although in the model a precipitated film is assumed to

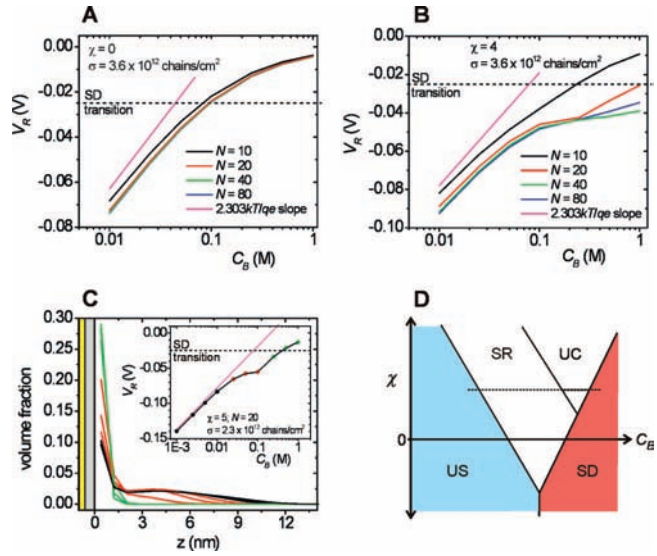

Figure 5. (A) Dependence of rest potentials on chain length in the absence of contact interactions, $\chi = 0$. (B) Dependence of rest potentials on chain length in the presence of chain-chain attractions, $\chi = 4$. (C) V_R response for a layer capable of both collapsed (high salt) and stretched (low salt) states of organization. (D) A classification map of V_R behaviors for the model, in C_B−χ space.

uniformly coat the solid support, incompatibility of the polyelectrolyte with solvent can lead to nonuniform coverage.[67,68] This possibility is not explored by the present model.

The dependence of V_R on chain length is considered in panels A and B of Figure 5 for $\chi = 0$ and 4, respectively. For $\chi = 0$ the layer does not collapse as there is no net preference for chain−chain over chain−solvent contacts, whereas for $\chi = 4$ a collapsed layer can exist. In both situations V_R becomes independent of N as chain length increases past 20 segments. This loss of sensitivity derives from the known result that, given a fixed number of chains per area, continued increase in the length of the chains must eventually be accompanied by a commensurate increase in film thickness, H, i.e., H must eventually scale linearly with N, $H \propto N$.[69,70] The linear relationship between H and N requires that the chain segment concentration $\phi_{segment} \approx \sigma N d^3/H$ lose its N-dependence and, since the concentration determines V_R, V_R also becomes independent of N.

The complex structure of the V_R−C_B traces for $\chi = 4$ in Figure 5B results from transitions in layer organization. Figure 5C provides a closer look at this type of scenario. At low salt the volume fraction profiles show the layer to be stretched (black curves) and the V_R response approaches US behavior (black points in the inset). An increase in salt concentration screens the electrostatic repulsions between chains, and allows the film to contract. This leads to SR behavior as indicated by the red points in the inset and red profiles in the main panel. Because of attractive segment−segment contacts the layer strongly contracts with increasing C_B until it precipitates onto the solid support (green profiles). The collapsed layer is not responsive to salt, leading to a UC state which transitions to the salt-

(67) Zhulina, E.; Singh, C.; Balazs, A. C. *J. Chem. Phys.* **1998**, *108*, 1175–1183.
(68) Sandberg, D. J.; Carrillo, J.-M. Y.; Dobrynin, A. V. *Langmuir* **2007**, *23*, 12716–12728.
(69) Alexander, S. *J. Phys. (Paris)* **1977**, *38*, 983–987.
(70) Halperin, A.; Tirrell, M.; Lodge, T. P. *Adv. Polym. Sci.* **1992**, *100*, 31–71.

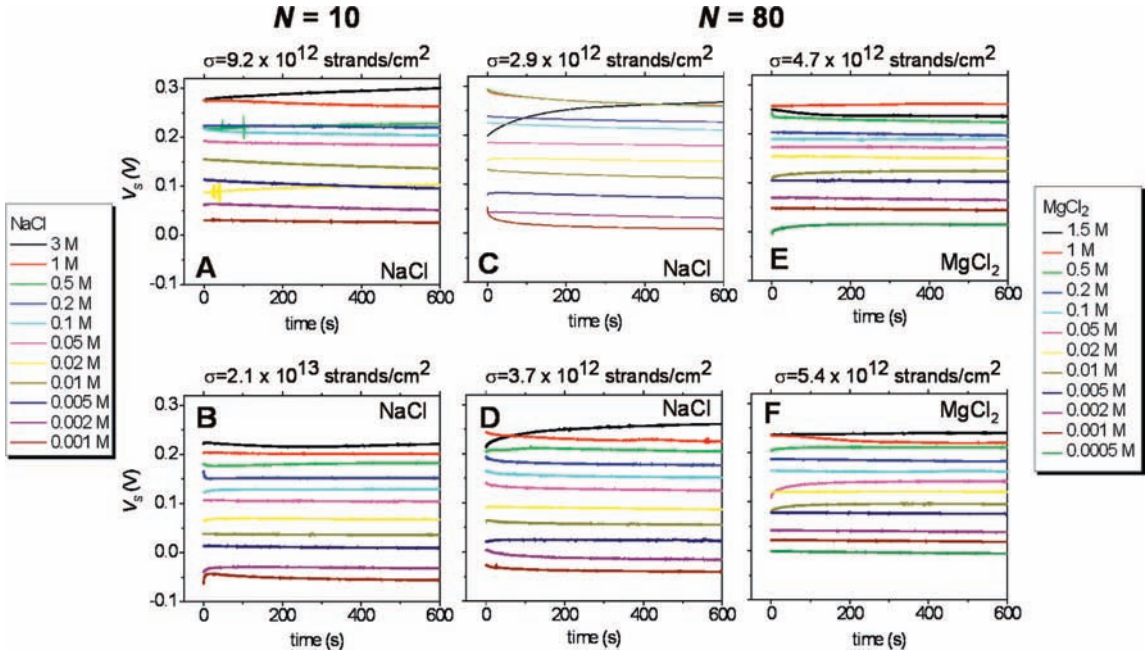

Figure 6. Time traces of open circuit potential, relative to Ag/AgCl wire reference, for 10mer polydT at two coverages in NaCl (A, B), 80mer polydT at two coverages in NaCl (C, D), and 80mer polydT at two coverages in $MgCl_2$ (E, F). The ionic strength series for NaCl measurements are shown at left; those for $MgCl_2$ are shown at right. In each case pH was adjusted to 7.0. For traces that stabilized the rest potential was obtained as the value at 600 s. All plots have identically scaled axes.

dominated regime at high salt (green points in the inset). This example illustrates that even for the relatively simple test model, as compared to the complexity of most experimental systems, the relationship between V_R and C_B can be nontrivial.

Figure 5D qualitatively summarizes conditions for US, SR, UC, and SD regimes in $C_B-\chi$ space. In the high salt limit the rest potential approaches zero in the SD regime, while in the opposite limit of infinitely dilute salt concentration the films swell and exist in the US regime. Between these two extremes any number of SR and UC regions could exist, depending on complexity of interactions. With a single χ value, one SR and one UC regime were observed, as discussed in the context of Figure 5C and as illustrated by the dashed path in Figure 5D.

3.3. Experimental Studies on polydT Monolayers. The ability of rest potential measurements to provide structural information, in the context of U, SD, and SR type responses described above but for an experimental system, was investigated for monolayers of polydT prepared on gold electrodes (Figure 1). PolydT monolayers are a homopolymer case of single-stranded DNA films widely used in DNA and RNA diagnostic applications,[8−10] whose fundamental properties and diagnostic performance are often investigated using gold-supported monolayers.[43,71−79]

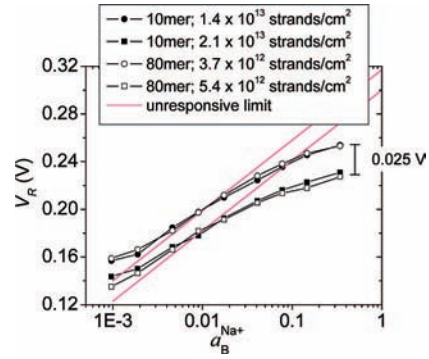

Figure 7. Experimental rest potentials V_R, expressed relative to Ag/AgCl/3 mol/L NaCl reference, as a function of solution Na^+ activity. Purple lines indicate the U-limit slope of 0.059 V per decade in ionic activity. The depicted range in activity corresponds to NaCl concentrations from 0.001 to 0.5 mol/L.

Experimental measurements determine the rest potential V_R from the stabilized (assumed equilibrium) value of the open circuit potential V_{OCP}. Examples of raw V_{OCP} data, prior to correction for dependence of the wire reference on Cl^- activity, are plotted in Figure 6. Achievement of a stable potential was favored by higher strand coverages (e.g., compare Figure 6A and B or Figure 6C and D) and by keeping salt concentrations below 1 mol/L. Under these conditions open circuit potentials relaxed toward stable signals over a few minutes. Only those conditions that yielded a stable potential within 600 s were analyzed further.

Rest potentials V_R, referenced to Ag/AgCl/3 mol/L NaCl as described in Materials and Methods, are plotted in Figure 7 as a function of Na^+ solution activity a_B^{Na+} for two coverages of 10mer and 80mer strands in NaCl electrolyte. For a fixed strand

(71) Peterson, A. W.; Wolf, L. K.; Georgiadis, R. M. *J. Am. Chem. Soc.* **2002**, *124*, 14601–14607.
(72) Dandy, D. S.; Wu, P.; Grainger, D. W. *Proc. Natl. Acad. Sci. U.S.A.* **2007**, *104*, 8223–8228.
(73) Lee, C. Y.; Gong, P.; Harbers, G. M.; Grainger, D. W.; Castner, D. G.; Gamble, L. *J. Anal. Chem.* **2006**, *78*, 3316–3325.
(74) Ricci, F.; Lai, R. Y.; Heeger, A. J.; Plaxco, K. W.; Sumner, J. J. *Langmuir* **2007**, *23*, 6827–6834.
(75) Baker, B. R.; Lai, R. Y.; Wood, M. S.; Doctor, E. H.; Heeger, A. J.; Plaxco, K. W. *J. Am. Chem. Soc.* **2006**, *128*, 3138–3139.
(76) Gorodetsky, A. A.; Ebrahim, A.; Barton, J. K. *J. Am. Chem. Soc.* **2008**, *130*, 2924–2925.
(77) Rant, U.; Arinaga, K.; Fujita, S.; Yokoyama, N.; Abstreiter, G.; Tornow, M. *Nano Lett.* **2004**, *4*, 2441–2445.
(78) Petrovykh, D. Y.; Kimura-Suda, H.; Whitman, L. J.; Tarlov, M. J. *J. Am. Chem. Soc.* **2003**, *125*, 5219–5226.
(79) Anne, A.; Bonnaudat, C.; Demaille, C.; Wang, K. *J. Am. Chem. Soc.* **2007**, *129*, 2734–2738.

length, an increase in surface coverage caused a negative shift in the rest potential. This downward shift is attributed to a rise in the surface concentration of negative polydT charge at higher strand coverage, σ. Interestingly, the four samples produced a similarly shaped response such that an ~4-fold lower coverage of 80mers resulted in potentials comparable to a 10mer layer of a higher coverage. Thus fewer longer strands per area were needed to generate a comparable concentration of strand charge at the surface. That the rest potentials are not just a function of strand coverage, but also of strand length, moreover indicates that these systems are not yet in the long chain limit discussed in connection with the lattice test model (Figure 5A and B).

The purple lines in Figure 7 represent an unresponsive layer for which, from eq 2, the slope is $2.303kT/q_+e$ per decade in Na^+ activity, or 0.059 V at 300 K. The closest that polydT layers come to unresponsive behavior is when a_B^{Na+} is around 0.005, but they never quite reach it. Rather, a weakened (more horizontal) dependence of V_R on a_B^{Na+} is observed both at high and low salt concentrations, indicating that cation activity in the layer a_F^{Na+} is adjusting so as to compensate changes in solution Na^+ activity. Starting from the high salt end, at sufficiently high concentrations the SD regime is anticipated. In the lattice model this regime spanned V_R between −0.025 and 0 V, with V_R converging to 0 at high salt. In experiments V_R does not converge to a zero limit, however, due to offset introduced by use of a reference electrode. Even without precisely knowing the high salt limit, it is nevertheless clear from the data that the SD regime cannot start below 0.22 V (on the experimental V_R scale), given that its total width would span only about 0.025 V (eq 3). That deviations from unresponsive behavior occur over at least 0.06 V in Figure 7, as a_B^{Na+}decreases down toward 0.005, therefore indicates structural responsiveness over most of this concentration range. Moreover, the enhanced deviation from a U-type response below a_B^{Na+} of 0.005 must be similarly due to an SR mechanism, since these potentials are ~0.09 V below the high salt value and thus far outside the possibility of salt-dominance.

At present we can offer only a partial interpretation of above trends in terms of molecular mechanisms. The responsiveness above a_B^{Na+} of 0.005 is attributed to changes in layer swelling due to electrostatic interactions between strands, qualitatively similar to behavior seen in the test model of the previous section. However, it is puzzling that, even at high salt, there is a persistent downward shift in V_R with strand coverage, since in this limit the membrane potential should begin to be suppressed with concomitant convergence of data for different σ. An additional unanswered question is the origin of the low salt responsiveness of the layer. Since neither of these trends were observed in the lattice model, the implication is that the responsible mechanisms were absent from that calculation. The low salt responsiveness, below a_B^{Na+} of 0.005, could derive from a number of effects. Two possibilities that could be examined experimentally are changes in strand-surface interactions (e.g., by using different alkanethiol passivation layers), and in the degree of strand ionization (e.g., by conducting experiments as a function of pH). The pronounced offset in rest potential, under high salt, could be a signature of layer nonuniformity. Under high salt, electrostatic repulsions between strands are diminished and attractive base-stacking and hydrogen-bonding interactions are likely to cause strand association.[80] Such aggregation would be expected to produce coverage-dependent extents of surface patchiness, with higher coverages leading to thicker, more uniform films and more negative V_R values.

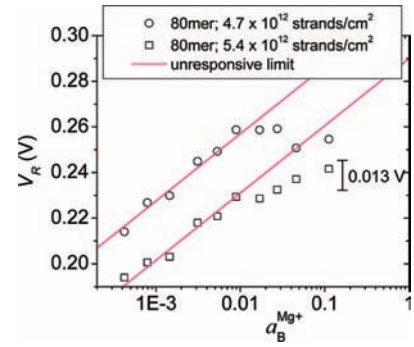

Figure 8. Experimental rest potentials, in $MgCl_2$ electrolyte. Purple lines represent unresponsive behavior. The range in activity corresponds to $MgCl_2$ concentrations from 0.5 mmol/L to 0.5 mol/L.

Substituting divalent Mg^{2+} for monovalent Na^+ cations, using $MgCl_2$ salt, produced a rather different rest potential response as shown in Figure 8. As salt concentration decreased from 0.5 mol/L to 0.5 mmol/L $MgCl_2$ an unresponsive state was reached around a_B^{Mg2+} of 0.01, with the predicted slope of $2.303kT/q_+e$ = 0.03 V per decade in Mg^{2+} activity. In contrast to the results in NaCl, there was no evidence for a responsive state at lower salt concentrations. For the lower coverage of 4.7×10^{12} strands/cm^2, a fairly sharp transition from an asymptotic high salt value of about 0.26 V to the unresponsive state was observed. Data from the 5.4×10^{12} strands/cm^2 coverage are also consistent with a rather narrow transition, with a width comparable to the 0.013 V potential span predicted for the SD regime from eq 3. The $MgCl_2$ results can therefore be summarized by a transition from an SD to an unresponsive U state as salt concentration is lowered. Similar to the trend in NaCl, an increase in strand coverage produced a downward shift in V_R.

Why would a U state, in which activity of Mg^{2+} in the film is largely independent of its value in solution, be observed? Multivalent counterions are known for their ability to precipitate polyelectrolytes from solution[81,82] as well as to collapse polyelectrolyte films[7,83,84] for example, by acting as electrostatic "cross-links" in which a single counterion attracts several polyelectrolyte charges. This propensity could lead to an unresponsive collapsed (UC) state, which would not be possible with monovalent Na^+ counterions. However, in addition to counterion multivalency, it is important to recognize the impact of specific chemical interactions.[85] In the case of Mg^{2+}, experimental[86] and theoretical[87] evidence has implicated the O4 and N3 of thymine as chelation sites toward this cation. This favorable and specific association would be a key contributor toward stabilization of a UC state. Our results in $MgCl_2$ moreover agree with recent sum frequency generation (SFG) spectroscopy experiments on single-stranded, dry DNA mono-

(80) Gong, P.; Levicky, R. *Proc. Natl. Acad. Sci. U.S.A.* **2008**, *105*, 5301–5306.
(81) Olvera de la Cruz, M.; Belloni, L.; Delsanti, M.; Dalbiez, J. P.; Spalla, O.; Drifford, M. *J. Chem. Phys.* **1995**, *103*, 5781–5791.
(82) Wittmer, J.; Johner, A.; Joanny, J. F. *J. Phys. II France* **1995**, *5*, 635–654.
(83) Jiang, T.; Wu, J. Z. *J. Phys. Chem. B* **2008**, *112*, 7713–7720.
(84) Mei, Y.; Lauterbach, K.; Hoffmann, M.; Borisov, O. V.; Ballauff, M.; Jusufi, A. *Phys. Rev. Lett.* **2006**, *97*, 158301.
(85) Hud, N. V.; Polak, M. *Curr. Opin. Struct. Biol.* **2001**, *11*, 293–301.
(86) Liu, H.; Sun, J.-L.; Hu, Y.; Han, K.-L.; Yang, S. *Chem. Phys. Lett.* **2004**, *389*, 342–347.
(87) Rincon, E.; Jaque, P.; Toro-Labbe, A. *J. Phys. Chem. A* **2006**, *110*, 9478–9485.

layers.[88] Based on SFG evidence, the authors in that study concluded that single-stranded DNA films were more structurally compacted after being exposed to Mg^{2+} than when monovalent counterions were used.

4. Conclusions

Rest potential (V_R) measurements offer a simple approach for investigating the states of organization in polyelectrolyte films. A general classification of V_R data is possible based on unresponsive (U), salt-responsive (SR), and salt-dominant (SD) behaviors. A U type response is characterized by a layer organization that is not sensitive to external solution conditions and for which the counterion activity in the layer is constant. In this situation, a linear relationship exists between V_R and log a_B^{ci}, where a_B^{ci} is the activity of the counterion in solution, with a slope of $2.303kT/qe$ where q is the counterion valence. In the SD regime the membrane potential between the layer and external solution is strongly suppressed—more specifically, the electrostatic work to transfer counterions between the layer and solution is less than the thermal energy kT. A perturbation in solution salt therefore results in a net transfer of ions so as to maintain the layer and solution activities comparable. In contrast, SR behavior is characterized by responsiveness of the layer structure to salt conditions. Similar to an SD state, for an SR regime the activity of counterions in the layer also adjusts to changes in solution activity; however, for an SR regime the adjustment primarily derives from a response of the polyelectrolyte film (e.g., swelling) rather than from ion transfer.

The above classification scheme was tested on theoretical and experimental data from layers of end-tethered polyelectrolytes. A lattice test model with adjustable contact interactions exhibited all three (U, SD, and SR) behaviors and suggested a further subdivision of the U regime into unresponsive collapsed (UC) and unresponsive stretched (US) states. The subdivision delineates origins of unresponsiveness as arising from overpowering attractions between chains (UC regime) or from saturation of chain elasticity (US regime). Experimental results on polythymidylic acid (polydT) monolayers in NaCl solutions indicated existence of two SR regimes in the range 0.001 to 0.5 mol/L salt. An unresponsive regime was not observed. In contrast, under divalent $MgCl_2$ electrolyte in the range 0.0005 to 0.5 mol/L, an unresponsive regime existed at lower salt concentrations that appeared to directly transition to SD behavior at high salt. The existence of a UC state for polydT films under $MgCl_2$ is consistent with known, specific associations between Mg^{2+} and thymine.

A major experimental challenge is to map regions of responsive behavior onto underlying molecular mechanisms. Presence of several responsive processes could obscure observation of clear-cut transitions or, alternately, lead to observation of more than one transition in V_R-C_B curves. Possible responses include layer swelling, changes in the extent of polyelectrolyte ionization, adjustments in lateral homogeneity of the layer, changes in polyelectrolyte/surface interactions (e.g., from image charges), and ion pairing or other effects arising from specific chemical affinities or the surface dielectric environment.

Acknowledgment. The described work was supported by the National Science Foundation under Award No. DMR 07-06170. The authors are grateful to Brian Olmsted for assistance with analysis of the surface roughness of gold-coated slides.

Supporting Information Available: Detailed explanation of lattice theory calculations and XPS data analysis; complete ref 7. This material is available free of charge via the Internet at http://pubs.acs.org.

JA807435Q

(88) Asanuma, H.; Noguchi, H.; Uosaki, K.; Yu, H.-Z. *J. Am. Chem. Soc.* **2008**, *130*, 8016–8022.